DOI: http://dx.doi.org/10.15446/ing.investig.v39n2.67604

Removal of acetylsalicylic acid (ASA) in packed microcolumns with carbon xerogel modified with TiO_2 nanoparticles

Remoción de ácido acetilsalicílico (ASA) en microcolumnas empacadas con xerogel de carbono modificado con nanopartículas de TiO_2

Viviana E. Gómez[1], Adriana P. Herrera[2], and Jorge H. Sánchez[3]

ABSTRACT

The adsorption capacity of acetylsalicylic acid was evaluated using carbon xerogel (CX) and carbon xerogel modified with TiO_2 nanoparticles (CXM). These materials were characterized by different techniques such as Scanning Electron Microscopy (SEM), X-Ray Diffraction (XRD), and Fourier Transform Infrared (FTIR) spectroscopy. BET surface area measurements found values of 762 m^2/g and 214 m^2/g for CX and CXM, respectively. Batch experiments show that the Langmuir-Freundlich model best represents the experimental adsorption isotherm, in addition to show a maximum adsorption capacity of 17,48 mg/g. In continuous experiments, the effect of the inlet concentration and flow rate on the adsorption capacity of the micro-packed bed adsorber were evaluated. Breakthrough curves agree well with the axial dispersion model. In view of their adsorption capacity, carbon xerogels provide a potential material for the removal of emergent contaminants from the pharmaceutical industry. Besides, the incorporation of TiO_2 nanoparticles allows the implementation of complementary techniques, e.g. photodegradation, as an alternative to achieve higher elimination of aqueous contaminants.

Keywords: Acetylsalicylic acid, Microcolumns, Nanoparticles, Titanium dioxide, Carbon xerogel.

RESUMEN

Se evaluo la capacidad de adsorcion de acido acetil salicılico usando xerogel de carbon (XC) y xerogel de carbon modificado con nanopartıculas de TiO_2 (XCM). Estos materiales se caracterizaron mediante tecnicas como la microscopıa electronica de barrido (SEM), difraccion de rayos X (DRX) y espectroscopia infrarroja (FTIR). Para el area superficial BET, se encontraron valores como 762 m^2/g para XC y 214 m^2/g para XCM. Los experimentos de adsorcion muestran que el modelo que mejor representa la isoterma es el de Langmuir-Freundlich, ya que mostro una capacidad de adsorcion maxima de 17,48 mg/g. En los experimentos en continuo, se evaluo el efecto de la concentracion de entrada y la velocidad del flujo sobre la capacidad de adsorcion del adsorbente en el lecho microempacado. Las curvas de ruptura concuerdan bien con el modelo de dispersion axial. En vista de su capacidad de adsorcion, los xerogeles de carbono son un posible material para la eliminacion de contaminantes emergentes de la industria farmaceutica. Ademas, la incorporacion de las nanopartıculas de TiO_2 permite la implementacion de tecnicas complementarias, por ejemplo, la fotodegradacion, como una alternativa para lograr una mayor eliminacion de contaminantes acuosos.

Palabras clave: Acido acetil salicılico, Microcolumnas, Nanopartıculas, Dioxido de titanio, Xerogeles de carbon.

Received: September 8th, 2017
Accepted: May 24th, 2019

Introduction

In recent years, a lot of waste is generated from industrial and human daily activities, producing toxic compounds that pollute the environment and cannot be degraded by nature. These residues include the so-called emerging contaminants (EC), which consist in a wide variety of chemical compounds, such as pharmaceutical drugs, personal care products, surfactants, plasticizers and chemical additives from industrial processes, that are not considered in the current monitoring programs for wastewater treatment (Jiang, Xiao, Wang, Wang, and Cai, 2015). Pharmacological residues represent the highest percentage of EC, which is a big concern for public health, since the effect of chronic exposure is unknown. (Tejada, Quiñonez, and Peña, 2014) One of the most commonly used drugs is the acetylsalicylic acid (ASA),

[1]Chemical Engineer and M.Sc. in Engineering, Universidad Pontificia Bolivariana, Colombia. E-mail: vivianaeloisa.gomez@upb.edu.co
[2]Chemical Engineer, Universidad de Cartagena, Colombia. M.Sc. and Ph.D. in Chemical Engineering, Universidad de Puerto Rico, Puerto Rico. Affiliation: Full-Professor, Universidad de Cartagena, Colombia. E-mail: aherrerab2@unicartagena.edu.co
[3]Chemical Engineer, Universidad Pontificia Bolivariana, Colombia. M.Sc. in Chemical Engineering, Universidad Nacional de Colombia, Colombia. Ph.D. in Chemical Engineering, Universidad de Puerto Rico, Puerto Rico. Affiliation: Full-Professor, Universidad Pontificia Bolivariana, Colombia. E-mail: jorgeh.sanchez@upb.edu.co

How to cite: Gómez, V. E., Herrera, A. P., and Sánchez, J. H. (2019). Removal of acetylsalicylic acid (ASA) in packed microcolumns with carbon xerogel modified with TiO_2 nanoparticles. *Ingeniería e Investigación*, *39*(2), 11-20. DOI: 10.15446/ing.investig.v39n2.67604

which serves as anti-inflammatory, analgesic, antipyretic and antiplatelet agent (Mukherjee, Ray, and Barghi, 2016). There are various methods for the removal of this type of contaminant from wastewater (Roig Bondia, 2013), but adsorption on carbonaceous materials appears to be the best and the most frequent strategy used, since it is efficient, economic, and environment-friendly (Vargas, 2013). Among these materials, there is a group called carbon xerogels, which have a mesoporous structure and are able to adsorb larger molecules, such as emerging contaminants or dyes (Álvarez, Ribeiro, Gomes, Sotelo, and García, 2015). In the literature, some studies have focused on the use of carbon xerogels as adsorbent materials. For example, Álvarez et al. (2015) studied the elimination of caffeine and diclofenac using carbon xerogels. The maximum adsorption capacity was 182,5 mg/g for caffeine and 80,0 mg/g for diclofenac. Carabineiro, Thavorn-amornsri, Pereira, Serp and Figueiredo (2012) used activated carbon, carbon nanotubes and carbon xerogel for the adsorption of ciprofloxacin, obtaining adsorption capacities from 112 to 135 mg/g. The carbon nanotube sample was the material with the highest adsorption capacity per unit area, which was attributed to its high surface area and electron-donor capacity.

The modification of the adsorbent material with TiO_2 nanoparticles offers additional advantages. Some of them are a synergistic effect with the adsorbent compound, through the increase of surface area as a function of the reduced particle size; the development of mesopores; the exposure of a more active crystalline phase; and the possibility of the subsequent photodegradation of the pollutant, avoiding the generation of residual products (Bailón-García et al., 2017; López-Muñoz, Arencibia, Cerro, Pascual, and Melgar, 2016). Authors such as Borges, García, Hernández, Ruiz-Morales and Esparza, (2015) studied the removal of paracetamol using a photoreactor, where TiO_2 was supported in glass spheres. The photocatalytic activity reached a high photodegradation between 99% and 100% after 4 hours of irradiation. Additionally, Bailón-García et al. (2017) studied a series of carbon xerogels-TiO_2 composites that were used as photocatalysts and adsorbents of dyes. They concluded that the adsorption of the dye is controlled by the mesopore volume, which augmented with the increasing percentage of titanium oxide present in the carbonaceous composite.

In the last two decades, related studies on the implementation of microdevices have shown that they have several advantages on conventional processes. Their small size and large surface to volume ratios leads to a lower driving force required for mass and heat transfer, thus smaller unit volumes are necessary (Kenig, Su, Lautenschleger, Chasanis, and Grünewald, 2013). Few studies about adsorption in microchannels have been reported. For instance, El-Qada, Abdelghany and Magdy (2013) studied the adsorption of dyes in a fixed-bed microcolumn using activated carbon. Their results show the effect of initial dye concentration, column diameter and particle size on the microcolumn performance. Sharma and Tiwari (2016) studied the removal of Cu^{2+} using acrylamide-co-maleic acid in a fixed-bed microcolumn. From these experiments, they observed that an increase in the flow rate and inlet concentration of the metal also increased the adsorption capacity up to a 98% of Cu^{2+}, with the possibility of bed regeneration for a new application.

In this work, we report the removal of acetylsalicylic acid using activated carbon xerogels modified with TiO_2 nanoparticles. Batch adsorption experiments were performed to obtain the equilibrium curves and determine the effect of the adsorbent dose, pH of the solution, and initial concentration of the adsorbate. Additionally, breakthrough curves were obtained for continuous removal using packed-bed microcolumns at different operating conditions.

Experimental

Reagents

Acetyl salicylic acid (ASA) was purchased from Sigma-Aldrich in analytical grade (> 99%). Formaldehyde (37% in water, stabilized with 10% methanol), resorcinol (≥ 99%) and sodium hydroxide (98%) were purchased from Merck. Titanium (IV) isopropoxide (95%) and tetraethyl orthosilicate (98%) were acquired from Alfa Aesar, while dimethylsulfoxide (99%) was obtained from Panreac.

Synthesis of carbon xerogel

Following the experimental procedure proposed by Álvarez et al. (2015), carbon xerogel (CX) was obtained by polycondensation of resorcinol with formaldehyde (molar ratio 1:2). In a typical experiment, 9,91 g of resorcinol was dissolved in distilled water, with the addition of 13,5 mL of formaldehyde solution. In order to achieve the desired initial pH of the precursor solution (pH = 6,1), sodium hydroxide solution was added drop wise under continuous stirring and pH monitoring. Later, the resulting solution was taken to an oven at 85 °C for 3 days. The obtained gel was then dried in an oven for several days at 60 °C, with a pressure ranging between 103 Pa and 105 Pa. Finally, the gel was calcined in the presence of N_2 at 900 °C for one hour and activated with CO_2 at 840 °C for 2 hours.

Synthesis of nanoparticles and modification of the xerogel

The synthesis of titanium dioxide (TiO_2) nanoparticles was performed using the green chemistry method, where a chemical reduction of titanium tetraisopropoxide was made using an aqueous extract obtained from leaves of lemongrass. For this synthesis, 850 mL of lemongrass extract were mixed with 1,33 mL of titanium tetraisopropoxide, shaking at 175 rpm for 24 hours. Afterward, nanoparticles were precipitated by centrifugation at 5000 rpm and dried at room temperature. To obtain the desired crystal structure, the TiO_2 nanoparticles were calcined at 450 °C for 3 hours. To modify the xerogel with the nanoparticles, 1,0 g of the carbonaceous material was initially prepared and suspended in 20 mL of organic solvent dimethylsulfoxide (DMSO), which was kept under slow shaking for 24 h at 30 °C. Then, 3 mL of tetraethylorthosilicate (TEOS) were added to the mixture

and left for 48 h at room temperature. Subsequently, 0,5 g of the synthesized nanoparticles were added to the suspension, and the mixture was placed on an orbital shaker for 12 hours at 30 °C. Afterward, the modified material was precipitated using a centrifuge at 5000 rpm for 15 min and then washed with ethanol (Bitar Castro and Mejía Meza, 2015).

Characterization of nanoparticles and carbon xerogels

The physicochemical, morphological and surface properties of the carbonaceous materials and TiO_2 nanoparticles were characterized by Scanning Electron Microscopy (SEM) in a JCM-6000 Plus microscope (JEOL Ltd, Japan). BET surface area measurements were taken in an ASAP2020 Plus System (Micromeritics, USA) and X-Ray Diffraction (XRD) was performed using Empyrean Series II X-ray diffractometer (Malvern Panalytical, USA). Finally, Fourier transform infrared spectroscopy was made in a Shimadzu Model IRAffinity-1S FTIR.

Dose curve

Carbon xerogels quantities between 25 and 250 mg were taken and put in contact with 25 mL of ASA aqueous solution, with concentration of 100 mg/L. The solution pH was not adjusted. The suspensions were continuously agitated at room temperature, at 150 rpm, for 7 h until equilibrium was reached. Then, suspensions were filtered, and the ASA equilibrium concentrations were determined at λ = 280 nm, using a UV-1800 spectrophotometer (Shimadzu, Japan). The removal efficiency at equilibrium was calculated using Equation (1).

$$\% \text{ removal} = \frac{\left(C_o - C_{eq}\right)}{C_o} \times 100 \tag{1}$$

where C_o (mg/L) is the liquid-phase concentration of ASA at $t = 0$ and C_{eq} is the equilibrium concentration.

Effect of solution pH

The pH of the experimental solutions was adjusted from 2 to 11 by addition of HCl and NaOH solutions. The ASA concentration was fixed at 100 mg/L. Tests were carried out at room temperature and agitated at 150 rpm with a contact time of 7 h. Once this time was elapsed, suspensions were filtered, and the ASA concentrations were determined at λ = 280 nm, using a UV-1800 spectrophotometer (Shimadzu, Japan).

Adsorption isotherms

Batch adsorption studies allow to obtain the equilibrium data for a fixed temperature of the mixture. In this test, different ASA solutions were prepared at concentrations between 10 and 200 mg/L, at room temperature. The doses of adsorbent and pH of the solution were taken from the previous results. After a contact time equivalent to 2 h, the solutions were filtered and analyzed in a UV-1800 spectrophotometer (Shimadzu, Japan) at a wavelength of 230 nm. This determined the adsorption of ASA on the evaluated material (Gómez Rengifo, 2013). Mass of ASA adsorbed per mass of each utilized material q_e, calculated according to Equation (2), is presented as a function of the ASA concentration C_e.

$$q_e = \frac{(C_o - C_e)\, V}{m} \tag{2}$$

where C_o and C_e (mg/L) represent the initial and the equilibrium concentration of the adsorbate in the solution, respectively. $V(L)$ is the volume of the solution, and m(g) is the dry mass of the adsorbent.

Langmuir (Eq. 3), Freundlich (Eq. 4) and Langmuir-Freundlich (L-F) (Eq. 5) adsorption models were used to fit the experimental equilibrium adsorption data (Álvarez et al., 2015).

$$q_e = \frac{q_{\max} K_L C_e}{1 + K_L C_e} \tag{3}$$

$$q_e = K_F\,(C_e)^{n_F} \tag{4}$$

$$q_e = \frac{q_{\max} K_L\,(C_e)^n}{1 + K_L\,(C_e)^n} \tag{5}$$

where C_e (mg/L) represents the equilibrium concentration in the aqueous phase, q_e (mg/g) the equilibrium adsorption capacity and $q_{\max}$ (mg/g) the maximum adsorption capacity according to Langmuir and Langmuir-Freundlich models. K_L (L/mg) is a parameter related to the adsorption intensity for Langmuir and Langmuir-Freundlich equations and n is a constant associated with the heterogeneity of the adsorber in the Langmuir-Freundlich model. K_F (L/g) and n_F are parameters that define the adsorption capacity and adsorption intensity in the Freundlich model. The parameters of the models can be estimated by nonlinear regression analysis, minimizing the following objective function (Eq. 6):

$$F.O. = \sum_{i=1}^{N} \left(q_{e,i\,\exp} - q_{e,i\,\mathrm{mod}}\right)^2 \tag{6}$$

Packed-bed microcolumn experiments

A capillary glass tube of 1,0 mm internal diameter and 10 cm length was used as adsorption microcolumn. The adsorbent material was ground and sieved to obtain an average particle diameter of 300 µm, which was packed in the column with a bed length of 5 cm. Solutions of different concentrations of ASA (50, 100 and 150 mg/L) were continuously fed into the microcolumn at different flow rates (0,5, 0,75 and 1,0 mL/min) using a NE-1000 syringe pump (New Era Pumps, USA). The change in time of the ASA concentration in the column effluent was determined by continuous UV measurements at a wavelength λ = 230 nm in a UV-1800 spectrophotometer (Shimadzu, Japan). The column was kept at room temperature. The microcolumn performance was evaluated through the breakthrough curves of the continuous fixed bed system and the adsorption capacity of the adsorbent. The latter is defined as the ratio of the total adsorbed contaminant in the bed

to the total amount of the adsorbent material packed in the column (Eq. 7).

$$A.C.\,(mg/g) = \frac{Q}{m}\int_0^t (C_i - C_e)\,dt \tag{7}$$

where Q (mL/min) is the feed flow rate, m (g) is the mass of the adsorbent, C_i (mg/L) is the influent concentration, C_e (mg/L) is the effluent concentration and t(min) is the adsorption time. For comparison purposes, the breakthrough point was taken at 10 % of the initial concentration. Additionally, breakthrough curves were fitted with the axial dispersion model (Eq. 8), which assumes a dispersed plug flow through the bed characterized by an axial dispersion coefficient.

$$\frac{C_e}{C_i} = \frac{1}{2}\left\{1 + \text{erf}\left[\left(\frac{uL}{4D_L}\right)\left(\frac{V - V_{\min}}{(VV_{\min})^{1/2}}\right)\right]\right\} \tag{8}$$

where erf(x) is the error function of x, u is the interstitial velocity of the fluid, D_L is the axial dispersion coefficient, V is the volume of the fluid sent to the packed-bed in an elapsed time, $V_{\min}$ is the minimum volume required to saturate the bed and L is the bed length. The model parameters D_L and $V_{\min}$ were determined by nonlinear regression analysis (Arango Cárdenas, 2015).

Results and Discussion

Characterization of TiO2 nanoparticles and carbon xerogels

FTIR analysis was used to identify functional organic groups on the surface of carbon xerogels and TiO_2 nanoparticles. The FTIR spectra are shown in Figure 1. CX shows peaks between 3600-3200 cm^{-1} due to the O-H stretching vibrations, which is characteristic of the presence of surface hydroxylic groups and chemisorption of water. Vibrations of the ring C=C=O between 2183-2160 cm^{-1} and 1751-1581 cm^{-1} were also observed, which can be attributed to the stretching vibrations of C=O moieties in carboxylic structures. The band at 1700 cm^{-1} can be related to the stretching vibrations of C=O from an unreacted aldehyde group and/or to the carbonyl generated when formaldehyde undergoes a ring-opening reaction (Álvarez et al., 2015). The bands near 1473 and 1435 cm^{-1} were assigned to the C-H stretching vibrations in organic structures, Moreover, bands at 1300-1000 cm^{-1} and 933-920 cm^{-1} can be related to the C-O-C vibrations of methylether bridges in the resorcinol molecules and tri-substituted benzene rings, respectively (Girgis, El-Sherif, Attia, and Fathy, 2012; Rodrigues et al., 2012; Álvarez et al., 2015).

For carbon xerogel modified with TiO_2 nanoparticles, a peak at 3695 cm^{-1} was observed (Fig. 1). This band can be attributed to the Ti-COOH between the nanoparticles and carbon material. Bands between 2978 and 2870 cm^{-1} correspond to the presence of alkenes, carboxylic acids, secondary amines and phenols, whereas bands between 1188-910 and 1 581 cm^{-1} are associated with the presence of the Ti-O-C bond. Likewise, bands between 1728-1600 cm^{-1} correspond to the vibrations of stretching and flexion of hydroxyl groups bound to titanium Ti-OH atoms, whereas between 1489-1435 cm^{-1} are bands corresponding to CH_3 deformation (Bitar Castro and Mejía Meza, 2015; Fornaris Lozada, 2015; Hudlikar, Joglekar, Dhaygude, and Kodam, 2012; Santhoshkumar et al., 2014). CXM shows peaks between 2877-2401 cm^{-1} and 686 cm^{-1} corresponding to the presence of alkenes, C-N and C-H groups. Bands at 2360 cm^{-1} and 2993 cm^{-1} are related to the presence of carboxylic acids and aromatic or aliphatic C-H groups. Bands at 3780, 1589 cm^{-1}, 1481-1422 cm^{-1}, and 1094-779 cm^{-1}, are associated to hydroxyl group adsorbed in the sample, the presence of Ti-O-C group and the CH_3 deformation, respectively. These peaks demonstrate that the carbon xerogel was effectively modified with TiO_2 nanoparticles.

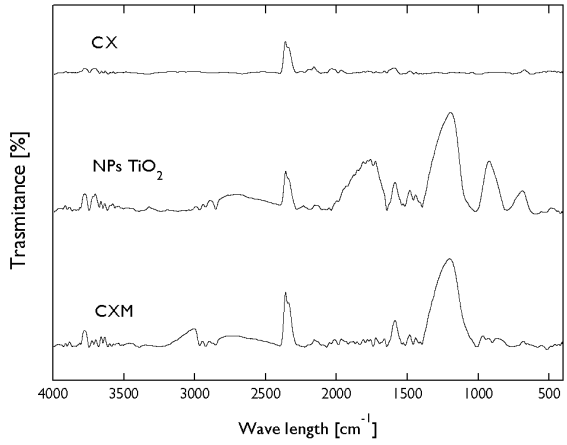

Figure 1. FTIR analysis for carbon xerogel, TiO_2 nanoparticle and carbon xerogel modified.
Source: Authors

Since carbon xerogels are mesoporous materials, Table 1 shows values about texture and porous structure of the carbonaceous materials considered in this study. Values of S_{BET} and porous parameters are higher than those obtained by Álvarez et al. (2015) for carbon xerogels, which could be due to the physical activation of the material. However, the surface area is similar to the one found for activated carbons, that is, between 824 and 1 237 m^2/g (Páez et al., 2012). Likewise, the surface area for TiO_2 nanoparticles agrees with those reported in literature of 116-586 m^2/g (Bailón-García et al., 2017; Zhou, Zhang, and Liu, 2012). Additionally, the lower S_{BET} for the modified materials is attributed to the presence of TiO_2 nanoparticles, since microporosity is mainly associated with the carbon phase (Bailón-García et al., 2017).

Table 1. Textural and porous parameters for carbon xerogel, TiO_2 nanoparticle and carbon xerogel modified with nanoparticles

	AS_{BET} (m^2/g)	$V_{mic.}$ (cm^3/g)	$d_{mic.}$ (nm)	$V_{meso.}$ (cm^3/g)	V_{Total} (cm^3/g)
CX	762	0,320	1,26	0,74	1,050
NPs- TiO_2	218	0,095	2,29	0,11	0,206
CXM	214	0,096	2,1	0,20	0,297

Source: Authors

Figure 2 shows the scanning electron micrographs (SEM) of carbon xerogel, TiO_2 nanoparticles and modified carbon xerogel. It is observed that nanoparticles are agglomerated, with a rounded structure and different sizes (Figure 2a). Activated carbon xerogel exhibits a smooth surface with a non-homogeneous particle size distribution, in addition to the formation of macropores, where TiO_2 nanoparticles can be deposited and ASA molecules adsorbed in the removal process (Figure 2b). For the modified carbon xerogel (Figure 2c), the micrographs show TiO_2 nanoparticles uniformly distributed on the surface of the material. These results agree with some previous studies, such as those by Álvarez et al. (2015), and Herrera, Reyes and Colina-Márquez (2016), where SEM images exhibit similar morphologies.

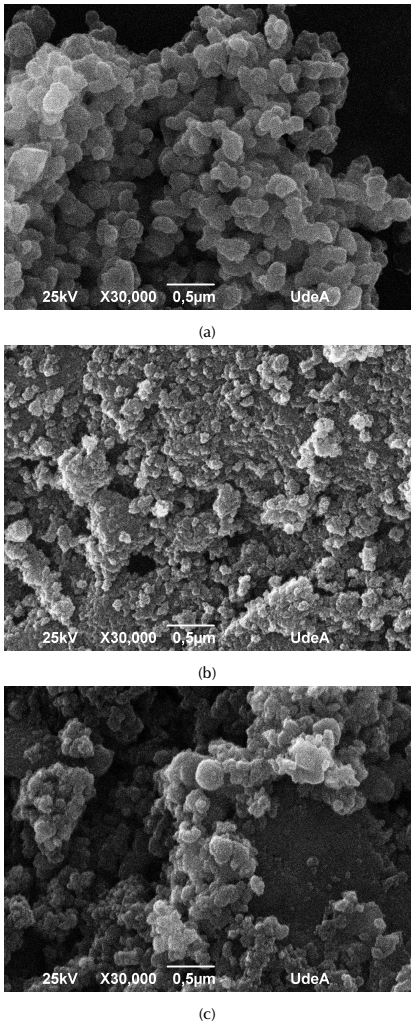

Figure 2. SEM-EDS results for a) nanoparticles of TiO_2; b) carbon xerogel; c) carbon xerogel modified with nanoparticles.
Source: Authors

The XRD technique allows the identification of the phases present in a sample and their degree of crystallinity. Figure 3 shows the results of XRD for TiO_2 nanoparticle and carbon xerogel modified. Peaks at 2θ = 25°, 30°, 48°, 50°, 54°, 55° and 62° correspond to the anatase phase, while peaks at 44° and 64° can be related to the rutile phase. The polymorph anatase form has a metastable characteristic, it is the most photoactive form of TiO_2, and it is widely studied due to their technological importance in various applications (Keane, 2013).

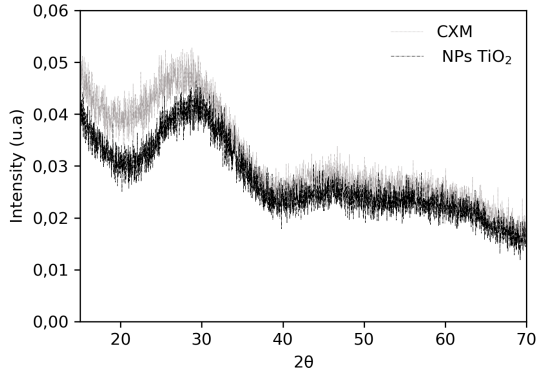

Figure 3. X-ray diffraction analysis for TiO_2 nanoparticles and carbon xerogel modified with TiO_2.
Source: Authors

Batch experiments

Dose curve and pH effect: The dose curve (Figure 4) shows an increase in ASA removal as the amount of CX increases, until reaching a maximum removal percentage of 91,82 % for an optimal dosage of 4,0 g/L.

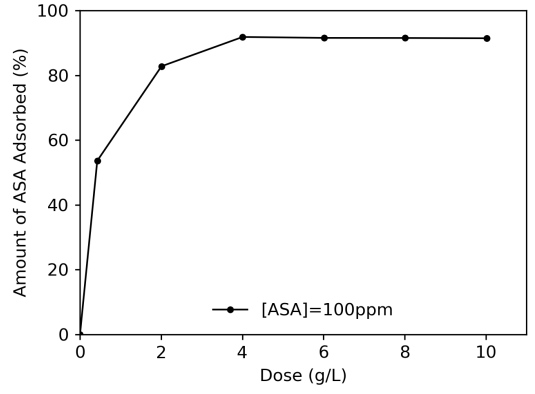

Figure 4. Effect of carbon xerogel dosage on the adsorption of ASA. Initial concentration = 100 mg/L; solution volume = 25 mL; time = 7 h; agitation speed = 150 rpm.
Source: Authors

The effect of the solution pH on the adsorption of ASA by CX is shown in Figure 5. The solution pH is a significant parameter that affects the adsorption process, as it alters the degree of ionization of the functional groups on the carbon surface. The adsorption capacity decreases with an increase in the solution pH. It has been suggested by Beninati, Semeraro, and Mastragostino (2008) that at low values of pH, the surface of the CX is positively charged, which produces an attractive force of the ASA anion, considering phenomena such as chemical bond, π-π-type interactions,

and electrostatic interactions related to the amphoteric nature of the carbons. As the pH of the ASA solution increases, a proportional decrease in adsorption takes place, probably due to the successive deprotonation of positive charged groups on the adsorbent surface and a subsequent electrostatic repulsion between ASA and the negatively charged sites on the adsorbent. There also exists a competition between OH (at high pH) and ASA for the remaining positively charged adsorption sites (Mphahlele, Onyango, and Mhlanga, 2015).

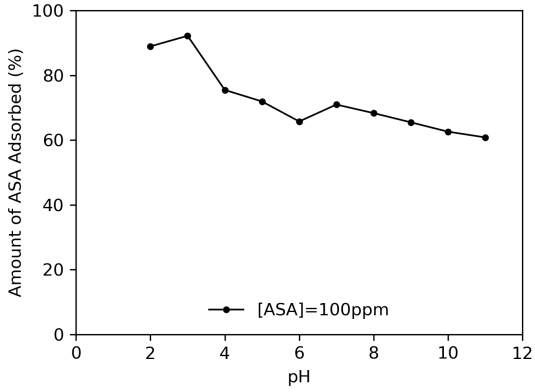

Figure 5. Effect of the solution pH on the adsorption of ASA. Initial concentration = 100 mg/L; solution volume = 25 mL; time = 7 h; agitation speed = 150 rpm.
Source: Authors

Adsorption isotherms: The adsorption isotherm describes the equilibrium relationship between bulk activity of the adsorbate in solution and adsorbed on the surface of the adsorbent at constant temperature (Pal, Deb, Deshmukh, and Verma, 2013). Figure 6 shows adsorption isotherms of ASA on carbon xerogel and carbon xerogel modified with TiO_2 nanoparticles. According to the classification system proposed by Giles, MacEwan, Nakhwa and Smith (1960), the isotherms for CX (Figure 6a) and CXM (Figure 6b) would correspond to the S class sub-group IV, given the initial slope and the shape of the upper part of the curves. This type of isotherms is typical for mesoporous materials, which indicates that adsorption becomes easier as ASA concentration raises. This also evidence that water molecules contribute negatively to adsorption, as they compete with ASA for active sites on surface. Likewise, the curve appears in sub-group IV, which is characterized by the development of a fresh surface where adsorption can occur, probably due to re-orientation of molecules already adsorbed (Álvarez et al., 2015; Giles et al., 1960).

Table 2 shows the fitting parameters of the Langmuir, Freundlich and Langmuir-Freundlich models (Equations 3-5) to experimental data. According to the correlation coefficient R^2, the adsorption of ASA onto CX and CXM is better fitted by the Langmuir-Freundlich model. This type of isotherm considers the heterogeneity of the solid surface, and is one of the models that best represents the removal of emerging contaminants (Álvarez et al., 2015).

Table 2. Parameters of Langmuir, Langmuir-Freundlich (L-F) and Freundlich models for ASA

Models	Parameters	CX	CXM
Langmuir	q_{max} (mg/g)	19,00	13,90
	K_L (L/mg)	$6{,}56\text{x}10^{-6}$	$2{,}01\text{x}10^{-6}$
	R^2	0,970	0,902
L-F	q_{max} (mg/g)	17,48	12,38
	K_L (L/mg)	$4{,}86\text{x}10^{-3}$	$2{,}50\text{x}10^{-4}$
	n	1,84	1,69
	R^2	0,991	0,972
Freundlich	n_F	1,17	1,54
	K_F (L/g)	1,09	$7{,}88\text{x}10^{-2}$
	R^2	0,990	0,972

Source: Authors

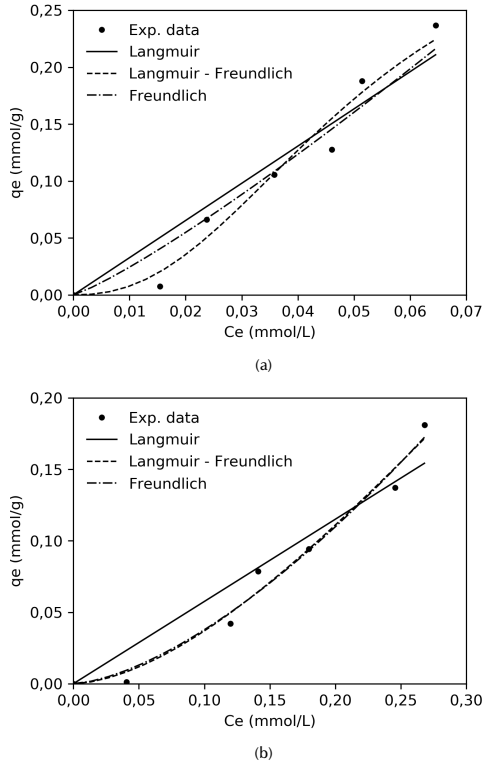

Figure 6. Adsorption isotherm of ASA onto (a) carbon xerogel and (b) modified carbon xerogel. C_o = 10-200 mg/L; xerogel dose = 4 g/L solution volume = 25 mL; pH = 3; T = 30 °C; t = 2 h.
Source: Authors

The maximum adsorption capacity (q_{max}) for CX and CXM was 17,5 mg/g and 12,4 mg/g, respectively. The lower adsorption capacity of CXM may be due to the micro- and meso-porosity blockage by TiO_2 nanoparticles, which is confirmed from results of porous parameters (Table 1). This fact denotes a preferential adsorption of ASA on the carbon surface, as found by Bailón-García et al. (2017) for the adsorption of orange G dye on TiO_2-carbon xerogel composites. Some of the functional groups of ASA that can occupy the available active sites on the surfaces of CX and CXM are aromatic

rings, through a charge transfer, and groups -OH and -OOH, by means of electron donation (Rakić, Rajić, Daković, and Auroux, 2013).

Continuous experiments

Breakthrough curve of acetylsalicylic acid: Results for the breakthrough curves at different feed conditions are shown in Figures 7 and 8. On the one hand, Figure 7 evidence that increasing the ASA feed concentration makes the bed saturation process faster. This fact may be attributed to an increase of the driving force for the mass transfer of the adsorbate from the bulk of the fluid phase to the solid phase, enhancing the adsorption rate. However, the microcolumn packed with CXM (Figure 7b) saturates sooner than the one packed with CX (Figure 7a) for the same concentration feed. This is likely due to the presence of TiO_2 nanoparticles that hinder the adsorption of ASA molecules, as was exposed in the batch experiments. Furthermore, the breakthrough curve for CXM shows a rather slow approach toward $C/C_o = 1$ asymptote, which is a well-known characteristic of particle-controlled systems. This fact is a consequence of the enhanced external mass transfer exhibited by microdevices and the low porosity of the material.

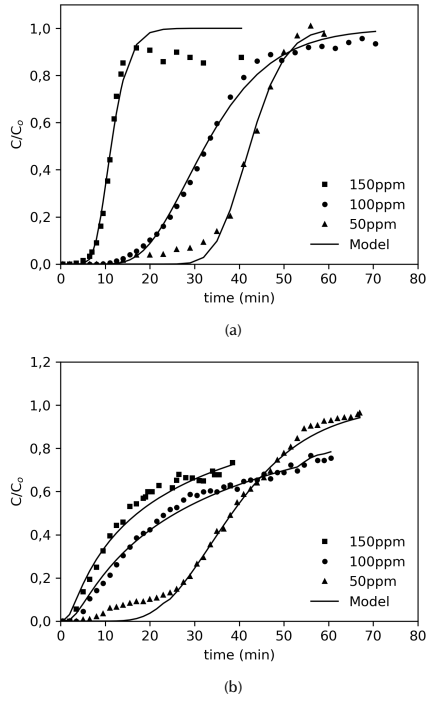

Figure 7. Breakthrough curves for ASA adsorption on (a) CX and (b) CXM for different feed concentrations. C_o = 50, 100, 150 mg/L; Q = 0,75 mL/min.
Source: Authors

On the other hand, Figure 8 shows that increasing the feed flow rate leads to a steeper breakthrough curve, since contact time between solution and solid is too short, resulting in a reduction in the breakthrough time. In this case, the solute has not enough time to interact with the surface of the adsorbent and diffuse into the pores, particularly

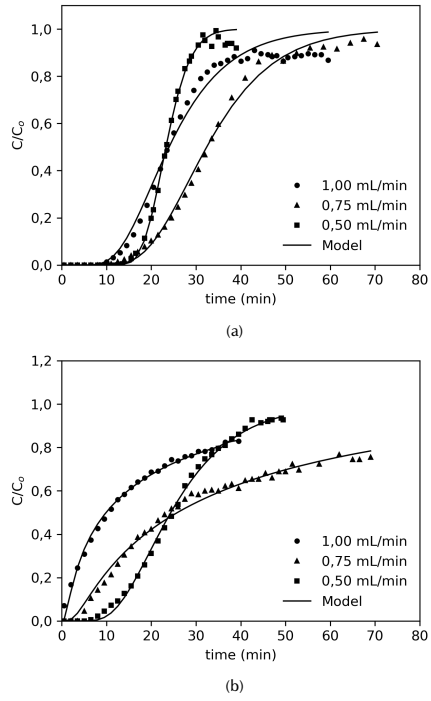

Figure 8. Breakthrough curves for adsorption of ASA on (a) CX and (b) CXM for different volumetric flows. C_o = 100 mg/L; Q = 0,5, 0,75 , 1,0 mL/min.
Source: Authors

with large molecules such as those of organic compounds, thus adsorption is limited (Cabrera-Lafaurie, Román, and Hernández-Maldonado, 2015). This behavior is more evident in the CXM sample (Figure 8b) than in the CX sample (Figure 8a), which could also be explained by the TiO_2 blocking active sites.

Table 3 summarizes the experimental results for breakthroughtime and adsorption capacity of the microcolumns, as calculated from Equation 7. The adsorption capacity was compared with the results obtained from the adsorption isotherms, $q_{\max}$. A significant decrease can be observed in $< z$ the amount of ASA retained by the xerogels. This can be explained by the fact that during the batch experiments, the CX and CXM samples had more contact time with the ASA solution, in addition to the constant stirring. This favored the interaction with the active sites and enhanced the mass transfer rate.

Equation 8 was used to fit the experimental breakthrough data. A summary of the estimated parameters, $V_{\min}$ and D_L, is presented in Table 4. It is observed that in most cases the correlation coefficient R^2 is higher than 0,99, indicating that an axial dispersion model is appropriate to describe well the breakthrough data. Furthermore, the axial dispersion coefficient increases with the volumetric flow rate in both adsorbents, obtaining in the sharpest breakthrough curves. Additionally, this indicates that there is an important contribution of the convection in flow direction. Finally, microcolumns packed with CXM exhibit higher values of D_L, which demonstrates a poor retention of ASA on this material.

Table 3. Experimental results of the continuous adsorption process

Q (ml/min)	C_I (ppm)	Breakthrough time (min) (C/Co = 0,1)	Mass of adsorbent (g)	Adsorption capacity (mg/g)
CX				
1,00	100	15,10	0,900	5,42
0,75	100	19,90	0,890	4,45
0,5	100	18,17	0,901	3,08
0,75	50	32,40	0,887	0,37
0,75	150	8,40	0,883	8,42
CXM				
1,00	100	0,92	0,901	5,28
0,75	100	6,40	0,901	3,60
0,50	100	12,88	0,901	2,87
0,75	50	19,90	0,901	0,39
0,75	150	4,40	0,904	6,69

Source: Authors

Table 4. Parameters of the axial dispersion model

Q (ml/min)	C_I (ppm)	V_{min} (mL)	D_L (cm^2/s)	R^2
CX				
1,00	100	23,97	21,06	0,983
0,75	100	24,29	13,47	0,994
0,5	100	11,64	4,60	0,996
0,75	50	31,76	5,52	0,992
0,75	150	8,49	10,37	0,924
CXM				
1,00	100	9,90	79,11	0,993
0,75	100	19,39	48,78	0,985
0,5	100	12,18	11,37	0,997
0,75	50	28,42	13,61	0,992
0,75	150	12,93	51,97	0,962

Source: Authors

Conclusions

The removal of acetylsalicylic acid (ASA) was studied using carbon xerogel and carbon xerogel modified with TiO_2 nanoparticles. It was found that low pH values favor the adsorption of ASA due to the positive charge of the carbon surface. The equilibrium experimental data for the CX and CXM were well fitted by the Langmuir-Freundlich model, where the maximum adsorption capacity of ASA was 17,48 mg/g and 12,38 mg/g for CX and CXM, respectively. Continuous experiments show that when increasing the inlet concentration and volumetric flow, breakthrough times are lower. In addition, the maximum adsorption capacities of the microcolumns were 8,42 mg/g for CX and 6,69 mg/g for CXM. Breakthrough curves agree well with the axial dispersion model. Results obtained from both equilibrium and continuous operation, demonstrate that the CXs could be used as a potential material to remove emerging contaminants such as ASA. Finally, despite experiments were not performed, the incorporation of TiO_2 nanoparticles would allow the subsequent elimination of the contaminant using a process of photodegradation, when exposed to UV or visible light, as shown by many authors in previous works such as Bailón-García et al. (2017), Zheng et al. (2018) and Ge, Zhang and Park (2019).

Acknowledgements

The authors are grateful to the Science, Technology and Innovation Department of Colombia (Colciencias) for the financial support (Grant No. 0208-2014) and the Universidad Pontificia Bolivariana (UPB), Medellin Campus, for the scholarship granted to the Chemical Engineer Viviana Gómez during her study at the master's degree of the Engineering Program. The authors also thank the collaboration of the research groups Pulp and Paper from the UPB and Multifunctional Nanomaterials from the Universidad de Cartagena for their assistance with the experimental process.

References

Álvarez, S., Ribeiro, R. S., Gomes, H. T., Sotelo, J. L., and García, J. (2015). Synthesis of carbon xerogels and their application in adsorption studies of caffeine and diclofenac as emerging contaminants. *Chemical Engineering Research and Design*, *95*, 229-238. DOI: 10.1016/j.cherd.2014.11.001Arango

Cárdenas, D. I. (2015). Evaluación del proceso de adsorción de 2,4 diclorofenol en microtubos empacados con carbón activado. (Undergraduate thesis, Universidad Pontificia Bolivariana). Retrieved from: https://repository.upb.edu.co/bitstream/handle/20.500.11912/2483/Trabajo/,/%20final/,/%20-/,/%20Daniel/,/%20I/,/%20Arango20C.pdf?sequence=1

Bailón-García, E., Elmouwahidi, A., Álvarez, M. A., Carrasco-Marín, F., Pérez-Cadenas, A. F., and Maldonado-Hódar, F. J. (2017). New carbon xerogel-IiO$_2$ composites with high performance as visible-light photocatalysts for dye mineralization. *Applied Catalysis B: Environmental*, *201*, 29-40. DOI: 10.1016/j.apcatb.2016.08.015

Beninati, S., Semeraro, D., and Mastragostino, M. (2008). Adsorption of paracetamol and acetylsalicylic acid onto commercial activated carbons. *Adsorption Science & Technology*, *26*(9), 721-734. DOI: 10.1260/02636 1708788251349

Bitar Castro, N. M., and Mejía Meza, R. J. (2015). Adsorción de níquel y cadmio usando cáscaras de limón y naranja modificadas con nanopartículas de dióxido de titanio y alúmina. (Unpublished Undergraduate thesis, Universidad de Cartagena). Cartagena, Colombia.

Borges, M., García, D., Hernández, T., Ruiz-Morales, J., and Esparza, P. (2015). Supported photocatalyst for removal of emerging contaminants from wastewater in a continuous packed-bed photoreactor configuration. *Catalysts*, *5*(1), 77. DOI: 10.3390/catal5010077

Cabrera-Lafaurie, W. A., Román, F. R., and Hernández-Maldonado, A. J. (2015). Single and multi-component adsorption of salicylic acid, clofibric acid, carbamazepine and caffeine from water onto transition metal modified

and partially calcined inorganic–organic pillared clay fixed beds. *Journal of Hazardous Materials*, *282*, 174-182. DOI: 10.1016/j.jhazmat.2014.03.009

Carabineiro, S. A. C., Thavorn-amornsri, T., Pereira, M. F. R., Serp, P., and Figueiredo, J. L. (2012). Comparison between activated carbon, carbon xerogel and carbon nanotubes for the adsorption of the antibiotic ciprofloxacin. *Catalysis Today*, *186*(1), 29-34. DOI: 10.1016/j.cattod.2011.08.020

El-Qada, E. N., Abdelghany, E. A., and Magdy, Y. H. (2013). Utilization of activated carbon for the removal of basic dyes in fixed-bed microcolumn. *International Journal of Energy and Environment*, *4*(5), 815-824. Retrieved from: http://www.ijee.ieefoundation.org/vol4/issue5/IJEE_07_v4n5.pdf

Fornaris Lozada, L. F. (2015). Modificación de las biomasas manihot esculenta y discorea alata con nanopartículas de tio2 para la adsorción de plomo y níquel en soluciones acuosas. (Unpublished Undergraduate thesis, Universidad de Cartagena).

Ge, J., Zhang, Y., and Park, S. J. (2019). Recent advances in carbonaceous photocatalysts with enhanced photocatalytic performances: A mini review. *Materials*, *12*(12), 1916. DOI: 10.3390/ma12121916

Giles, C. H., MacEwan, T. H., Nakhwa, S. N., and Smith, D. (1960). Studies in adsorption. Part XI. A system of classification of solution adsorption isotherms, and its use in diagnosis of adsorption mechanisms and in measurement of specific surface areas of solids. *Journal of the Chemical Society*, 3973-3993. DOI: 10.1039/ JR9600003973

Girgis, B. S., El-Sherif, I. Y., Attia, A. A., and Fathy, N. A. (2012). Textural and adsorption characteristics of carbon xerogel adsorbents for removal of cu (ii) ions from aqueous solution. *Journal of Non-Crystalline Solids*, *358*(4), 741-747. DOI: 10.1016/j.jnoncrysol.2011.12.004

Gómez Rengifo, V. E. (2013). Adsorción binaria de cadmio y níquel empleando lignina de bagazo de caña de azúcar (Unpublished undergraduate Thesis, Universidad Pontificia Bolivariana). Medellín, Colombia

Herrera, A., Reyes, A., and Colina-Márquez, J. (2016). Evaluation of the photocatalytic activity of iron oxide nanoparticles functionalized with titanium dioxide. *Journal of Physics: Conference Series*, *687*(1),012034. DOI: 10.1088/1742-6596/687/1/012034

Hudlikar, M., Joglekar, S., Dhaygude, M., and Kodam, K. (2012). Green synthesis of TiO_2 nanoparticles by using aqueous extract of jatropha curcas L. Latex. *Materials Letters*, *75*, 196-199. DOI: 10.1016/j.matlet.2012.02.018

Jiang, W., Xiao, F., Wang, D. S., Wang, Z. C., and Cai, Y. H. (2015). Removal of emerging contaminants by pre-mixed pacl and carbonaceous materials. *RSC Advances*, *5*(45), 35461-35468. DOI: 10.1039/C5RA03183

DKeane, D. (2013). Evaluation of the performance of activated carbón and titanium dioxide composites for pharmaceutical adsorption and photocatalysis in water (Ph.D. Thesis, Dublin City University). Retrieved from: http://doras.dcu.ie/19281/

Kenig, E. Y., Su, Y., Lautenschleger, A., Chasanis, P., and Grünewald, M. (2013). Micro-separation of fluid systems: A state-of-the-art review. *Separation and Purification Technology*, *120*, 245-264. DOI: 10.1016/j.seppur.2013.09.028

López-Muñoz, M.-J., Arencibia, A., Cerro, L., Pascual, R., and Melgar, Á. (2016). Adsorption of Hg(II) from aqueous solutions using TiO_2 and titanate nanotube adsorbents. *Applied Surface Science*, *367*, 91-100. DOI: 10.1016/j.apsusc.2016.01.109

Mphahlele, K., Onyango, M. S., and Mhlanga, S. D. (2015). Adsorption of aspirin and paracetamol from aqueous solution using Fe/N-CNT/β-cyclodextrin nanocomopsites synthesized via a benign microwave assisted method. *Journal of Environmental Chemical Engieneering*, *3*(4), 2619-2630. DOI: 10.1016/j.jece.2015.02.018

Mukherjee, D., Ray, A. K., and Barghi, S. (2016). Mechanism of acetyl salicylic acid (aspirin) degradation under solar light in presence of a TiO_2-polymeric film photocatalyst. *Processes*, *4*(2), 13. DOI: 10.3390/pr4020013

Pal, J., Deb, M. K., Deshmukh, D. K., and Verma, D. (2013). Removal of methyl orange by activated carbon modified by silver nanoparticles. *Applied Water Science*, *3*(2), 367-374. DOI: 10.1007/s13201-013-0087-0

Páez, C. A., Contreras, M. S., Léonard, A., Blacher, S., Olivera-Fuentes, C. G., Pirard, J.-P., and Job, N. (2012). Effect of CO_2 activation of carbon xerogels on the adsorption of methylene blue. *Adsorption*, *18*(3), 199-211. DOI: 10.1007/s10450-012-9394-2

Rakić, V., Rajić, N., Daković, A., and Auroux, A. (2013). The adsorption of salicylic acid, acetylsalicylic acid and atenolol from aqueous solutions onto natural zeolites and clays: Clinoptilolite, bentonite and kaolin. *Microporous and Mesoporous Materials*, *166*, 185-194. DOI: 10.1016/j.micromeso.2012.04.049

Rodrigues, L. A., Campos, T. M. B., Alvarez-Mendes, M. O., Coutinho, A. d. r., Sakane, K. K., and Thim, G. P. (2012). Phenol removal from aqueous solution by carbon xerogel. *Journal of Sol-Gel Science and Technology*, *63*(2), 202-210. DOI: 10.1007/s10971-012-2745-3

Roig Bondia, J. (2013). Eliminación de contaminantes emergentes mediante humedales artificiales como sistema alternativo o complementario a un tratamiento de aguas convencional. (M.Sc. Thesis, Universitat Politécnica de Valéncia) Retrieved from: http://hdl.handle.net/10251/44470

Santhoshkumar, T., Rahuman, A. A., Jayaseelan, C., Rajakumar, G., Marimuthu, S., Kirthi, A. V., Arivarasan, V.K., Kanayairam, V., Thomas, J., and Kim, S.-K. (2014). Green synthesis of titanium dioxide nanoparticles using psidium guajava extract and its antibacterial and antioxidant properties. *Asian Pacific Journal of Tropical Medicine*, *7*(12), 968-976. DOI: 10.1016/S1995-7645(14)60171-1

Sharma, N., and Tiwari, A. (2016). Effective removal of Cu^{2+} ions from aqueous solution in fixed-bed micro column using nanomagnetite-loaded poly (acrylamide-co-maleic acid) hydrogel as adsorbent. *Desalination and Water Treatment*, *57*(10), 4523-4536. DOI: 10.1080/19443994.2014.991945

Tejada, C., Quiñonez, E., and Peña, M. (2014). Contaminantes emergentes en aguas: Metabolitos de fármacos. Una revisión. *Revista Facultad de Ciencias Básicas*, *10*(1), 80-101. DOI: 10.18359/rfcb.341

Vargas, D. P. (2013). Preparación, caracterización y funcionalización de materiales carbonosos para la adsorción de Co_2. (Ph.D. Thesis, Universidad Nacional de Colombia). Retrieved from: http://www.bdigital.unal.edu.co/39721

Zheng, X., Xu, S., Wang, Y., Sun, X., Gao, Y., and Gao, B. (2018). Enhanced degradation of ciprofloxacin by graphitized mesoporous carbon (GMC)-TiO_2 nanocomposite: Strong synergy of adsorption-photocatalysis and antibiotics degradation mechanism. *Journal of Colloid and Interface Science*, *527*, 202-213. DOI: 10.1016/j.jcis.2018.05.054

Zhou, W., Zhang, P., and Liu, W. (2012). Anatase TiO_2 nanospindle/activated carbon (AC) composite photocatalysts with enhanced activity in removal of organic contaminant. *International Journal of Photoenergy*, *2012*, 7. DOI: 10.1155/2012/325902